

---

# Quantifying stimulus-relevant representational drift using cross-modality contrastive learning

---

Siwei Wang<sup>1</sup>, Elizabeth A de Laittre<sup>2</sup>, Jason MacLean<sup>2,3</sup>, and Stephanie E Palmer<sup>1,4</sup>

<sup>1</sup>Department of Organismal Biology and Anatomy, University of Chicago

<sup>2</sup>Committee on Computational Neuroscience, University of Chicago

<sup>3</sup>Department of Neurobiology, University of Chicago

<sup>4</sup>Department of Physics, University of Chicago

## Abstract

The representational drift observed in neural populations raises serious questions about how accurate decoding survives these changes. In primary visual cortex, it is hotly debated whether such variation is a direct tuning shift that would corrupt decoding or if it can be explained by changes in behavioral or internal state, which could be compensated by joint encoding of the stimulus and the state. We estimate the effects of stimulus-relevant representational drift on decoding using a publicly accessible dataset of mouse V1 responses to a natural movie. Because the only invariant component of the sensory experience across all 24 animals is that they all watch the same natural movie, we can learn a subject-invariant efficient neural representation that retains only stimulus-relevant components. We use contrastive learning between the neural response and the stimulus to learn a neural representation for stimulus-relevant features. This learned representation minimizes decoding error as quantified by Bayes risk. We show that it can be used to read out behaviorally relevant stimulus features (time, static scene, optic flow, and joint spatio-temporal features) at 33ms resolution accurately, a finer timescale than what has previously been explored. When we use the model trained on one recording session to derive feature activations on another, decoding performance is reduced by approximately 40%. Motion encoding is most susceptible to representational drift. In addition, when we enlarge the error tolerance window to 1sec, we recover stable stimulus encoding across sessions, echoing previous findings. This shows that decoding stimulus features that vary on fast timescales may require complex computation downstream of V1 to compensate for representational drift. This approach is able to assess the decoding of different features in complex natural scenes and quantify drift flexibly. Future work may use it to understand representational drift at a broad range of timescales.

## 1 Introduction

As technology has improved, the neuroscience community has been able to record larger neural populations over longer periods of time, allowing us to investigate how neural encoding changes over time. Perhaps surprisingly, correlations of neural activity with stimulus and behavioral variables have been observed to change within the same animal from recording session to recording session, over a timescale of hours to days to weeks, in a wide range of sensory and association brain areas [40, 17, 58, 87, 38, 39]. Strikingly, in cases where animals have been trained on a task, the behavioral performance, which presumably relies on the representations of the stimulus, remains stable over the same timescale. This phenomenon of "representational drift" poses a neural coding conundrum: assuming that the task-relevant variables in question are read out from these neural

populations, how are downstream brain areas able to compensate for such drift? Determining whether and how different components of stimulus or behavior are stably encoded in neural activity can reveal mechanisms of information processing in the nervous system. For example, it has been demonstrated in many brain areas that stimulus and behavioral variables can be stably decoded at the population level in spite of day-to-day drift in the encoding properties of single neurons [80, 23, 22, 35, 87, 16, 73, 29, 50, 2, 20, 19, 9, 38, 60, 10, 43, 52, 61, 17, 53, 6], supporting hypotheses about distributed codes [62]. This understanding will be further informed by investigating how and why drift occurs in the first place. By digging into *which* encodings are drifting and over what timescales, we can shed light on the underlying causes of changing representations. Here we focus our attention on the population encoding of a naturalistic stimulus, comparing the encoding of multiple stimulus variables with different spatio-temporal properties. We demonstrate that the neural population encoding of these variables changes over time but differently for different variables.

We used publicly available recordings from mouse primary visual cortex (V1) from the Allen Brain Observatory to quantify representational drift in responses to a natural movie stimulus. We focus on Neuropixels recordings [32] from V1, in which animals viewed a 30 second clip from the movie "Touch of Evil" [11]. Through a contrastive learning approach, we learn a representation of neural activity that emphasizes the encoding of features of the natural movie, such as object texture or motion, and de-emphasizes subject- or session-specific information. We refer to this as a stimulus-relevant representation. To further reduce the influence of internal state and behavioral variables on the stimulus-relevant representation [54, 36], we combine neural data from multiple animals into "pseudomice," under the assumption that the majority of stimulus-irrelevant variables will be uncorrelated across mice. Thus through the contrastive learning paradigm we learn a representation of the neural activity that also highlights features of the stimulus encoding that are shared across animals.

Natural movies contain stimulus features that span a range of timescales, up to the frame rate of the movie (30Hz) [1]. The Neuropixels recordings have a 30kHz sampling frequency but are binned to 30Hz in this dataset. Representational drift may change the encoding of an external stimulus at all timescales. However, the majority of previous research on representational drift in V1 investigated neural encoding on a timescale of one second or longer [13, 40, 54], missing any effects of drift on visual processing of faster features [63, 30, 66]. We focus on decoding at single-frame resolution. As we will show later in the paper, features in the natural movie do indeed vary on such a short timescale, thus motivating investigation of V1 encoding at this temporal resolution.

It is prohibitively difficult to parameterize a natural stimulus; thus it remains unknown in fine detail how a V1 population processes natural movies. Learning a stimulus-relevant representation of the neural activity is a first step towards addressing this challenge in sensory neuroscience. In particular, it is unclear which components of complex natural stimuli are encoded in V1 population activity, so we use time in the natural scene (frame identity) as a proxy for the suite of spatio-temporal features present in the movie up to that moment. Previous studies have assumed a particular mapping from stimulus to neural activity, often linear [80, 13], but we know there is considerable nonlinear processing of natural stimuli in V1 [28, 26, 82].

To extract a parsimonious stimulus-relevant representation from neural population activity, we employ a task-agnostic contrastive learning approach, which has been successful in extracting robust representations in other domains. Early work on image-text pair training used a representation of images to predict words within their respective text descriptions or labels [64, 31, 69, 34]. Recent work leveraged the superior expressive power of modern architectures [15, 55, 84] to learn image representations from text. CLIP [48] is a prominent example of this approach; the model was trained on 400 million pairs of images and their corresponding text descriptions [59]. The resulting representations were shown to perform well in a variety of zero-shot classification scenarios. Recent papers [18, 51] have connected such efficiency to its approximation of the information bottleneck principle [72]. Similarly, we choose this task-agnostic contrastive learning approach here because it does not make explicit assumptions about the exact mapping of neural activity to the stimulus.

This dataset from the Allen Brain Observatory contains two recording sessions of natural movie stimulus presentation separated by 90 minutes. For the first session, we obtain a stimulus-relevant neural representation through two phases of contrastive learning [7, 8, 70]. In the first phase, we learned a general neural representation by contrasting neural activity from multiple animals occurring in the same time within a session, thus learning a representation shared by all animals. In the second

phase, we contrasted this representation with that for the natural movie, matching each single stimulus frame with neural activity that occurs in the same time window. We were able to near-optimally decode time in the natural scene (frame identity) from the learned representation of neural population activity. We further showed that this training paradigm improves the geometry in the representation space for linear decoding. This is a property of the training paradigm that does not have implications for the neural encoding. However, it allows us to use the learned representation as a feature extractor to understand what features became harder to linearly decode due to representational drift from session 1 to session 2. Although we, too, observe a stable natural movie representation when adhering to the broad timescale used in previous work [54, 40, 13], we also observe that multiple spatio-temporal features changing at fast timescales could not be read out from representations trained on session 1 but applied to session 2, indicating that the neural representation of these features has drifted.

## 2 Results

### 2.1 Learning a generalizable representation from cross-modality contrastive training

We use the publicly available recordings of mouse V1 responding to a natural movie within the Allen Brain dataset in this study. There are two sessions that are 90 minutes apart (shown in 1). We focus on the neural activity responding to a natural movie because previous work demonstrated a higher order magnitude of representational drift responding to natural movies versus gratings [40]. Because we are interested in stimulus-relevant neural responses at all the timescales including those at fast timescales, we focus on the Neuropixels recordings which samples the neural activity at 30Hz. This is the same as the frame rate of the natural movie. This dataset contains 30 trials in both sessions for 24 animals. Following [13], we create two pseudomice, each aggregated from 5 animals (totalling up to 340-390 V1 units) for subsequent analysis. When we learn a stimulus-relevant neural representation, we sample neural activity from a 330ms window (10 frames) centered at movie frame  $t$  (see supplementary method for details).

Because natural movies contain complex spatio-temporal features, we use a task-agnostic contrastive learning method to learn the neural representation of the natural movie. This contrastive learning method is based on multi-view contrastive learning [70]. Training consists of two phases. Phase I is the single-modality pretraining. In this phase, we learn separate representations for the neural activity and the natural movie. Phase II is the cross modality training phase. During Phase II, we first create a set containing all views from both modalities (e.g., the representation discriminates frame  $t$  from others by combining five views: neural activity from pseudomice 1 and 2, the frames  $t$  and  $t + 1$ , and the respective optic flow frame between  $t$  and  $t + 1$ ). Then we contrast between all possible pairs of modalities in this cross-modality set of views (see Fig 2 for details).

Given any two views  $z_1$  and  $z_2$ , we use the InfoNCE loss [75] to compute the contrastive loss with respect to  $z_1$ :  $\mathcal{L}_{InfoNCE} = \frac{1}{n} \sum_{j=1}^n -\log \left( \frac{\exp(s(z_{i,1}z_{i,2})/\tau)}{\sum_{i=1}^n \exp(s(z_{i,1}z_{j,2})/\tau)} \right)$ .

In the above InfoNCE loss,  $s(\cdot)$  is the similarity function [7, 8] (or a critic [70]) and the number  $n$  controls how many negative pairs are included. Intuitively, the contrastive learning method learns to pull "positive" pairs together (e.g., if they share the same label) and push "negative" pairs away [25, 77]. This objective can be viewed as a variational lower bound on the mutual information [75, 47] with a formal limit controlled by the  $n$  [42]. Recent work also interpreted this loss objective as the alignment of positive pairs with entropy regularization controlled by negative pairs [71]. This interpretation highlights that using a larger  $n$  will provide a better approximation for the entropy regularization term.

If both views come from the same animal (with the only difference being from random augmentation), the above InfoNCE loss corresponds to the contrastive loss used in self-supervised learning [7]. Considering that we have views from heterogeneous modalities (similar to [48, 84]), we instead use the symmetric version of the InfoNCE loss in both directions to train our models:  $\mathcal{L}_{z_1, z_2} = 1/2\mathcal{L}_{InfoNCE}(z_1, z_2) + 1/2\mathcal{L}_{InfoNCE}(z_2, z_1)$ .

Both training phases help the learned representation to encode time in the natural scene (frame identity), which serves as a proxy for other spatiotemporal features of the movie. The single-modality pretraining learns time by pulling neural activity between pseudomice A and B from the same time in the natural movie together and pushing apart neural activity from different times in the representation space. The cross-modality training learns time through additional contrastive pairs between neural activity and their respective frames. This is so-called "weak supervision" because we only construct

Decode time	Model <sub>neural</sub>	Model <sub>scene</sub>	Model <sub>flow</sub>	novel pseudomouse (neural)
single-modality	99.7%	95.8%	93.8%	97.7%
cross-modality	99.7%	96.0%	95.2%	98.1%

**Table 1: During both the pretraining phase and cross modality training phase, our trained neural backbones can decode time (frame identity) up to single frame resolution. The natural movie backbones can decode time at high accuracy as well. We also tested the neural backbone using neural activity from a novel pseudomouse (constructed from a distinct subsets out of the 24 mice available). This shows that the trained model is generalizable. Note that the neural backbone only receives supervision from the natural movie during the cross modality training phase.**

positive pairs by sampling them into the same data tuple. The loss function does not treat different data tuples within a minibatch from the same time window as positive pairs (including explicit label information into contrastive learning is full supervision, i.e., supervised contrastive learning; [33]). Table 1 shows that such weak supervision is sufficient for the encoders to learn to differentiate frame identity. We are able to decode time in the natural scene from neural representation at a 99% accuracy. Cross-modality training is successful at maintaining this high decoding performance. Moreover, we can generalize the learned representation to decode from a novel pseudomouse, at 97% decoding performance.

The high decoding performance we observed in Table 1 suggests that cross-modal contrastive training learns a near-optimal representation in the following sense. We define time in the natural scene as a decodable variable  $Y$ . If input is  $X$  ( $X$  can be neural activity, movie frame, optic flow, etc), Table 1 suggests that  $X$  may contain all available information about  $Y$ . This corresponds to having an encoder which can achieve  $R(Y|X) \rightarrow 100\%$  where  $R(\cdot)$  is the expectation of decoding loss, formally defined as the Bayes risk [78] for decoding  $Y$  (see supplementary for derivations). Considering that all our decoding are using a learned representation  $Z$  from  $X$ , we recognize that there is a Markov chain  $Z$ - $X$ - $Y$ , such that all information  $Z$  contains about  $Y$  comes from  $X$ . Therefore, the Bayes risk of decoding  $Y$  using  $Z$ , i.e.,  $R(Y|Z)$ , is bounded by the Bayes risk  $R(Y|X)$  from above [18]. Table 1 shows that  $R(Y|X) \geq 99\%$ . Knowing that the upper bound is 100%, this corresponds to  $R(Y|Z) = R(Y|X)$ . Because cross modality training maintains  $R(Y|Z) = R(Y|X)$ , we characterize the learned representation as an optimal representation that is generalizable despite shifts within probability distributions present in both neural and movie modalities (more formally, the covariate shift [5, 4], see Supplementary Information for derivations). In Fig 2, we illustrate that cross-modal contrastive learning obtains this optimal representation by emphasizing the shared partition (i.e., "support match") between modalities while maintaining the same Bayes risk.

## 2.2 The cross-modality training optimizes the representation of time in the natural scene for linear read out

Observing that all test performances remain high (as shown in Table 1) throughout single-modality pretraining and cross-modality training, we investigate here how support matching during cross-modality training reformats the geometry of the representation space. Considering that the performance of contrastive learning is typically evaluated via the performance of a linear classifier [8, 7, 79, 77, 33, 70, 3], we ask a particular question: Does cross-modal training improve the representation of time in natural scenes for better linear readout?

We use a recently discovered phenomenon, i.e., the Neural Collapse [45, 27, 86], that occurs pervasively in today’s deep net training paradigm (using cross-entropy [45], MSE [27], or contrastive losses [21]) to characterize the difference between cross-modal and single-modal training. Neural collapse occurs when a deep neural network is trained beyond training error plateaus, where additional training may still improve test performance. In our scenario, this corresponds to persistently maintaining optimal decoding performance. When neural collapse emerges, the last layer features collapse to their means. Given that there are  $C$  different time segments in our data, neural collapse in our training predicts that the activation for different time segments will collapse into  $C$  different means. These means for different time segments will also form a  $C$ -simplex equiangular tight frame (ETF) [65] in the representation space. As a result, linear classification between different time merely requires the classifier to find the nearest class mean. Theorem 3 in [45] describes why such a  $C$ -simplex ETF is optimal for linear classification.

Formally speaking, let activation  $h = \mu_c + \epsilon$ , where  $\mu_c$  is the mean of activations for samples belonging to class  $c \in \{1, \dots, C\}$  and  $\epsilon$  is the noise. In the scenario that the data is balanced (i.e., there are equal number of samples per class or  $c \sim \text{Unif}(1, \dots, C)$ , see Supplementary Information for details), these class means are code words for a linear classifier  $Wh + b$  to read out the class

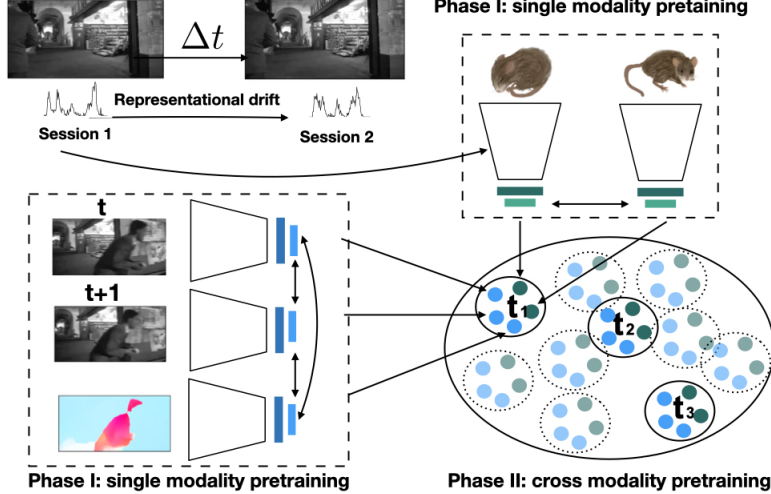


**Figure 1: Overview of encoding model.** We focus on the Allen Brain Observatory dataset that contains two sessions of Neuropixels recordings of "natural movie 1". There are 30 presentations of the movie per session. The time interval between sessions is  $\Delta t = 90\text{min}$ . We obtain a representation of neural activity that contains only stimulus-relevant features through two phases of contrastive training. In the first phase, we train on pairs sampled from different views within the same modality. In the neural modality, this corresponds to randomly sample a 330ms long window of neural activity from pseudomouse 1 and contrast it with another randomly sampled window of neural activity from pseudomouse 2. Sample pairs that correspond to the same time in the movie are positive samples in the contrastive learning framework (weak supervision by co-occurrence). In the natural movie modality, we contrast three views (frame  $t$ ,  $t+1$  and their corresponding optic flow frame) following previous work [68]. In the second phase, i.e., the cross modality training phase, we create a union of all views from both modalities. There are five views in total (pseudomouse 1, pseudomouse 2, frame  $t$ , frame  $t+1$  and optic flow frame). We then use pairwise contrastive learning to fine tune both the neural backbone and the natural movie backbones ( $\binom{5}{2}=10$  pairs total). Our goal is to learn a representation that pulls samples from any modality that correspond to the same time bin close together and pull apart samples that occur at different time bins (solid line circles represent different tuples that were pulled together for their respective time in the natural scene during training). We hypothesize that if we can learn an optimal representation that retains all discriminable information from session 1, then the difference between decoding performance between session 1 and session 2 is an estimate of how much stimulus-relevant representational drift occurs during the time interval (90 min) between these recording sessions [12, 63].

labels. Then a theorem introduced in [45] shows that these class means are optimal code words for classification if they form a  $C$ -simplex ETF

**Theorem 2.1** (Optimality of the  $C$ -simplex ETF for linear classification [45], see Supplementary Information for details). *Under the assumptions stated above (linear classifier and activations are class means with independent Gaussian noise), the optimal error exponent  $\beta$  is:*

$$\beta^* = \max_{M,W,b} \beta(M,W,b) \quad \text{s.t.} \quad \|\mu_c\|_2 \leq 1 \forall c$$

where  $\beta^*$  achieves its optimality at  $\frac{C}{C-1} \cdot \frac{1}{4}$  when  $M$  is the  $C$ -simplex ETF i.e.,  $M^* = \sqrt{\frac{C}{C-1}}(I - \frac{1}{C}\mathbb{1}\mathbb{1}^T)$

Note that the above theorem was introduced for full supervision (i.e., label information is included during training). This is different from our training dynamics, where only weak supervision is present (entries within a data tuple share the same time segment but not across different tuples). Nonetheless, Figure 3 shows that the cross-modality training leads to a representation closer to the  $C$ -simplex ETF compared to the initial single-modality pretraining representation. We show this as the diminishing of standard deviation between activation norms (here the activations are the means of samples belong to the same time segment) in Figure 3A) and that the angles between different activation means converge to the maximum angle ( $\cos^{-1}(\theta) = 1/(C-1)$ ,  $C = 400$  in Figure 3B (we also show the other two related neural collapse phenomena, i.e., variability collapse and classifier collapses to finding the nearest class mean in the Supplementary Information). In the extreme scenario, the learned neural representation with natural movie supervision would collapse into  $C$  different points. Each correspond to a different time segment in the movie. These time-relevant clusters would not contain any neural specific features that is not included in the natural movie. Therefore, we interpret a

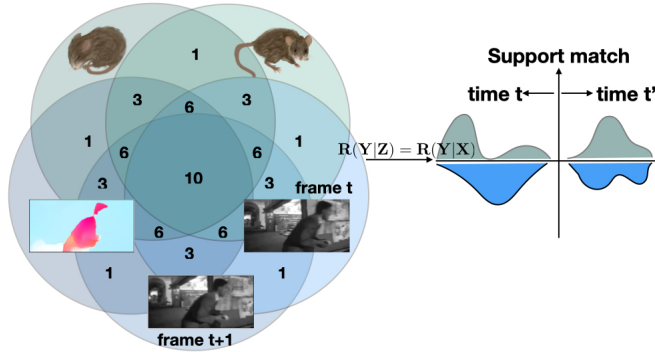


Figure 2: Cross-modality contrastive learning gives us a representation of neural activity that emphasizes the stimulus-relevant features it contains. This is because cross-modality contrastive learning enforces support matching between the two modalities, which can be thought of as an alignment of the representations learned for each modality in the Phase I pretraining. Because our decoding performance remains high (>99%) during both the single phase pretraining and cross-modality contrastive training (shown in Table1), we recognize that the Bayes risk relevant to decoding time is minimized. This minimization intrinsically matches the support across all the modalities during the cross-modality supervised contrastive learning phase. The left plot is the information diagram for the full graph contrastive paradigm. The numbers within the regions indicate how much "weight" the total loss assigns to each information partition (i.e., how many of the  $\binom{3}{2} = 10$  contrastive pairs includes the respective partition). It is obvious that the part shared by all the modality gets the highest weight. In the scenario that the Bayesian risk of the decoding remains optimal (i.e.,  $R[Y|Z] = R[Y|X]$ ), the emphasis of the partition shared by all modalities approximately becomes the support of representation across all modalities (Note that this approximation is not exact because all other partitions are getting less, but still positive weights). In the Supplementary Information, we formally derive this support match by defining cross-modality training as learning a neural representation optimal for retaining natural movie relevant features despite the distribution shift between neural and natural movie modalities [51]. Here we illustrate the support match as matching both the support and the discrimination boundaries between modalities (on the right).

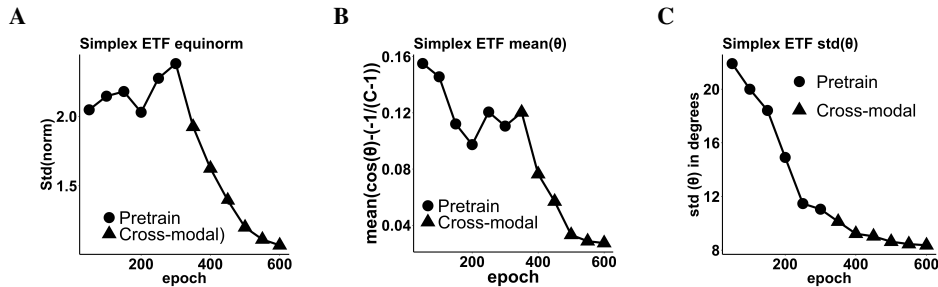


Figure 3: Cross-modality contrastive learning optimizes the representation of time (frame identity) for linear readout. This optimization is analogous to the terminal phase of training in other modern deep neural networks where further training still improves the representation even after decoding error gets close to zero. Means of activations for different time bins become  $C$ -simplex equiangular tight frame (ETF) ( $C=400$  in our model training, see Supplementary Information for training details). A simplex ETF geometry is a signature phenomenon that characterizes the optimal activations for linearly classifying these time bins as distinct categories [45]. When the training error goes stable or near zero (achieved during the pretraining phase) and training continues (during the Phase II cross modality supervised training), the deep neural network organizes all the class clusters to form a  $K$ -simplex ETF (here  $C=400$  as this is how many frames/distinct time labels we have). Such simplex ETF indicates first, that the means of activations for all classes have a similar norm (shown in A as the  $Std_{norm} = Std_c(\|\mu_c - \mu_G\|_2 / Avg(\|\mu_c - \mu_G\|_2))$  goes down); second, the mean angle  $\theta_{\mu_{c,c'}}$  between class means goes to the maximal angle  $\cos^{-1}(1/(C-1))$ . This was shown in [46] to be optimal for class separability (shown in B) and the standard deviation between angles  $std(\theta_{\mu_{c,c'}})$  also goes down (shown in C).

better C-simplex ETF (shown in Figure 3) as an evidence that the cross-modality training emphasizes stimulus-relevant components in learned neural representation.

### 2.3 Finding a rich set of stimulus-relevant features varying over different timescales

In this section, we investigate if there are stimulus-relevant features varying at different timescales that collectively represent time in the nature scene at the single frame resolution. Previous decoding approaches have mostly focused on changes in scene textures in the movie [80, 57], but recent experiment [41] also showed that motion-relevant information is present in V1. Therefore, we dissect the natural movie into a two-stream learning representation [70, 56, 24]. This is the same as how we set up the multi-view contrastive learning for natural movie in Section 2.1.

We performed two independent hierarchical clusterings: one on the frames themselves (static) and one on the optic flow frames (dynamic) of the test movie segment. If textures govern the discrimination between frames in both dynamic and static settings, then these clusterings should produce similar clusters. Before clustering, we converted all static frames and their corresponding optic flow frames to features that are the activation from the last ReLU layer in a ResNet50 trained with ImageNet [14]. This clustering was used in [76]. The difference here is that we did not try to minimize the mutual information between resulting clusterings of static scene and optic flow. Instead, we observe that both clusterings for scene and optic flow do not follow the temporal order (i.e., they do not keep increasing as time progresses). They represent time in the natural scene by assigning a distinct label to each frame. These labels vary at different timescales. Therefore, the Pearson correlation between time in the natural scene and any of these clusterings (scene, optic flow, or joint features) is low ( $\sim 0.05$ ). In addition, the Pearson correlation between optic flow labels generated by clustering and scene labels generated by clustering is as low as 0.02.

We also observe that the decay of autocorrelation in flow labels is much faster than that for labels from scene clustering, as shown in Figure 4, meaning that optic flow frames close to each other in time are less likely to have the same clustering label as their corresponding static frames. The decay for flow labels is as fast as 3 frames ( $\sim 100$  ms) as opposed to 15 frames ( $\sim 500$  ms) for the scene labels. We also observed zero-crossings in the autocorrelation of scene labels, which correspond to scene switches within the movie. By contrast, this natural movie clip has rather uniform and smooth camera movements, such that we do not observe zero-crossings in flow labels. We also observed a similar decay for the 400 frames in the second half of the movie (see Supplementary Information). In the subsequent section, we will train linear classifiers to read out these stimulus features. The weak supervision from the natural movie helps the learned representation of neural activity to solve a "pretext task" [83], i.e., discriminating time in the nature scene at the single frame resolution means the representation must retain information about stimulus features from multiple timescales. In this section, we test this hypothesis by reading out scene, flow, and the joint movie features that vary at different timescales. This is analogous to how previous work in contrastive learning evaluates the robustness of learned representations by reading out color information or rotation from a given image [7, 8, 33, 83].

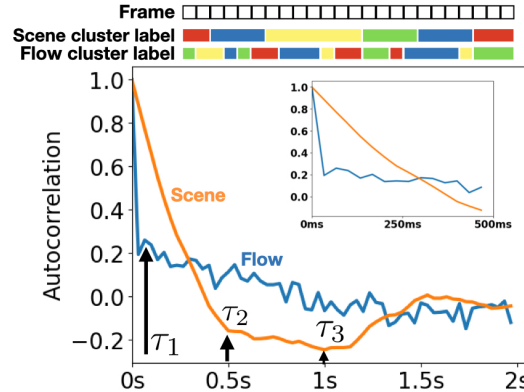


**Figure 4: Stimulus-relevant features of the natural movie vary over different timescales: textures in static frames ("scene") and optic flow. If we use the labels from the scene and optic flow clusterings to separately label the movie frames, we find that the autocorrelation in labels decays differently for scene and optic flow (schematized at the top, with actual data below). The optic flow labeling has a fast change, i.e., it decays to near zero after 66-100 ms (2-3 frames). On the contrary, the decay for scene labeling is much slower. It only reaches zero after 400 ms and reaches a negative peak around 1s (likely corresponding to scene change in the movie). This figure shows results for the first 400 frames (1st half of the movie), and we observe the same difference in decay timescales for the second half of the movie (see Supplementary Information). Note that because these clustering labels do not obey temporal order (they don't get bigger/smaller as time in the natural scene progresses), we find that the correlation between scene/flow/joint features and time are generally low (0.05-0.1). Therefore, these stimulus-relevant features are separable from time in the natural scene.**



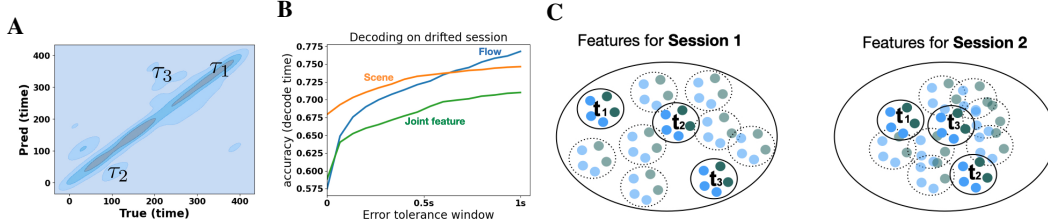


**Figure 5: The learned neural representation does not generalize to a different session of stimulus presentation.** A) The kernel density plot of the confusion matrix for decoding time (frame identity) from activations for session 2 neural data in the model trained on session 1 neural data (zero-shot). The peaks in this confusion matrix (i.e., the most likely errors) exhibit three different timescales. The shortest timescale of errors matches the dropoff in the flow label autocorrelation (shown in Figure 4). The mid and long timescales of errors correspond to decay in the scene label or scene switches in the natural movie. B) The change in decoding accuracy if we treat predicted labels as correct if they occur within a time window around the true label (e.g., if the time window is 1 second long, that means we will treat predicted labels as correct if it matches any of the true labels within  $\pm 15$  frames. In B),  $t = 1$  second means the frame occurs within the window  $[-500ms, 500ms]$  centered on the true label. C) Illustration on why the representational drift changes the read out of stimulus features. We hypothesize that representational drift may push clusters closer together and shuffle their positions from the original session. This shuffling is what makes reading out the proper stimulus features challenging. For example, in the left plot, reading out that  $t_3$  is different from  $t_1$  is transitive, i.e., we only need to know that  $t_1$  is different from  $t_2$  and  $t_2$  is different from  $t_3$ . In the right plot, we need to learn a separate decision that  $t_3$  is different from  $t_1$ . This added complexity may prevent the linear classifier from performing well even after training.

#### 2.4 Features that vary on fast timescales are the most susceptible to stimulus-relevant representational drift

Because we are able to decode both time in the natural scene and these stimulus-relevant features near optimally (the top row of 2), we use the trained model to estimate the magnitude of representational drift relevant to decoding between session 1 and session 2. When we linearly decode feature activation from session 2 with the model trained using neural representations from session 1, the degradation in decoding performance shows the impact of representational drift for encoding stimulus-relevant features. Table 2 shows that even after we retrain the linear classifier, we still see at least a 40% degradation in linear decoding performance. Representational drift seems to disrupt feature decoding at the 33ms, i.e., single-frame, timescale.

If we take a closer look at the confusion matrix for time in the natural scene (Figure 5A), we notice that the decoding errors seem to correspond to different decay timescales shown in Figure 4 (see Supplementary Information for additional results). This motivates us to define a noisier measure of accuracy if the decoder tolerates errors across a broad range of temporal windows. Previous work typically conducted decoding [13, 80, 57] within a one-second time window, which corresponds to training a decoder to identify which frame a given neural activity belongs to within  $pm$  15 frames. Using such a broad time window, previous observation suggested the stimulus representation was largely stable despite representational drift. If the decoder were to tolerate errors within a window up to  $\pm 15$  frames (a 1 second window), we would reproduce the stable stimulus representation previously observed. Figure 5B shows that the decoding accuracy of all spatio-temporal features goes up to 75% (72% for scene features and 82% for optic flow features) when we allow a 1 second error tolerance window. In particular, the decoding of motion features (i.e., optic flow) changes the most as we broaden the error tolerance window (orange line in Figure 5B). This also corresponds to our observation that the  $\tau_1$  error dominates the confusion matrix shown in Figure 5A. It is possible that the representational drift not only pushes encodings for different time segments closer (and hence more easily confused), but also shuffles the positions of different time segments in the representational space (illustrated in Figure 5C), which makes linear classification challenging even after training. Overall, we find that there indeed exists a stable stimulus representation at slow timescales. At fast timescales, motion-related features are much more susceptible to the representational drift between sessions.

### 3 Discussion

In this work, we introduce an encoder model that is able to learn a stimulus-relevant neural representation by contrasting neural activity and the corresponding natural movie stimulus. Because our learned representation minimizes the Bayes risk for decoding, we then use the trained model as a surrogate to investigate how the neural encoding of the natural movie changes over time. When comparing the



<b>Session 1 to 1 (Both pseudomice)</b>	<b>Time</b>	<b>Joint Feature</b>	<b>Scene</b>	<b>Flow</b>
Hold-out test	99.7%	99.9%	99.4%	99.8%
<b>Session 1 to 2 (Both pseudomice)</b>	<b>Time</b>	<b>Joint Feature</b>	<b>Scene</b>	<b>Flow</b>
zero-shot	46.2%	54.9%	47.4%	47.9%
trained linear classifier	67.5%	60.0%	69.3%	58.2%
<b>Session 1 to 2 (Pseudomouse 1 only)</b>	<b>Time</b>	<b>Joint Feature</b>	<b>Scene</b>	<b>Flow</b>
zero-shot	45.6%	44.6%	54.4%	47.1%
trained linear classifier	85.7%	71.5%	77.2%	69.3%

**Table 2: Representational drift with respect to the decoding of spatio-temporal features.** We include four spatio-temporal features: time, clustering on the static frames (scene), clustering on the optic flow frames (flow) and corresponding pairings of the scene and optic flow (joint feature). Zero-shot indicates that we use the linear decoders trained on the session 1 neural activity to decode these labels from the activations from the session 2 neural activity. Trained linear classifier means that we train a separate linear classifier on activations from session 2 neural activity. The contrastive learning models that generate these activations are trained on session 1 in both cases. If there is no representational drift, the decoding performance on the session 2 activations should be high, similar to the previous table. We show linear decoding performance using pseudomouse 1 alone (the performance of using pseudomouse 2 is similar, see Supplementary Information) as well as using both pseudomice together. Using both pseudomice gives worse performance than a single pseudomouse, indicating that the direction of representational drift is not necessarily coordinated across the pseudomice.

neural representation from session 1 with the neural representation for the same stimulus presented 90 minutes later in session 2, we observe a dramatic change in the representation, quantified by a drop in decoding performance for both dynamic and static stimulus features. If we tolerate a noisy readout such that the decoding is correct if the predicted spatio-temporal label is within 1 sec from the true label (similar to [40, 13, 57]), we recover previous findings that there exists a largely stable neural representation of the natural movie. However, we also find that the decoding of spatio-temporal features at fast timescales is more susceptible to representational drift.

This work contributes to a larger conversation about how best to quantify representational drift in neural population data, and in particular presents a new finding about *what* is changing in V1 encoding of natural movies rather than just *that* the encoding changes: the encoding for static features is relatively stable over the measured timescales, while the encoding for dynamic features (optic flow between frames) is less stable. If downstream brain areas were to read out features changing at fast timescales, it would be necessary to compensate for this drifting representation. For example, predictive mechanisms [49, 37, 44] may help downstream systems correct for this kind of drift in stimulus features.

Similar to other modeling approaches for neural populations [67, 85, 3, 57, 81], this method does not require the same cells to be tracked across sessions. It only assumes that the neural population is sufficiently sampled. In this dataset from the Allen Brain Observatory, none of the electrophysiological (neural) data is spike sorted (there is no attempt to separate the spiking activity of different neurons). Thus, it is most appropriate to treat this data using population approaches [74]. The main methodological difference between this work and others is that we optimize the learned representation for linear readout, while others optimize their representations for reconstructing neural activity [67, 85, 3, 57, 81]. We find that the learned representation retains a whole suite of spatio-temporal features varying at multiple timescales. They collectively encode time in the natural scene at the single frame resolution.

In the future, we plan to extend this work in several directions. First, we focused on the shortest possible timescale provided by the dataset. We used inductive bias such that both natural movie and neural activity are sampled at the same frequency to design learning with natural movie supervision. In the future, we hope to design new representation learning methods that bridge between modalities of different timescales through machine learning instead of hand engineering. Second, although we find that V1 encoding for the fast timescale stimulus features that could differentiate individual frames is less stable than the encoding for slower timescale stimulus features, using neural activity from only one cortical area limits our ability to understand if such unstable responses are being used downstream. If we can contrast neural activity from multiple areas, we may provide a more accurate answer on the influence of observed representational drift in V1 on behaviors. We also hope to use this learning paradigm to quantify representational drift at multiple timescales (e.g., hours to days to weeks) [36]. As the field develops longer-term tracking methods, this method will allow us to

compare neural representations across a range of intervals to disentangle the factors contributing to representational drift at fast versus slow timescales.

## References

- [1] Allen brain observatory – neuropixels visual coding. Technical report, 2019.
- [2] A. Arieli, A. Sterkin, A. Grinvald, and A. Aertsen. Dynamics of ongoing activity: explanation of the large variability in evoked cortical responses. *Science (New York, N.Y.)*, 273:1868–1871, Sept. 1996.
- [3] M. Azabou, M. G. Azar, R. Liu, C.-H. Lin, E. C. Johnson, K. Bhaskaran-Nair, M. Dabagia, B. Avila-Pires, L. Kitchell, K. B. Hengen, W. Gray-Roncal, M. Valko, and E. L. Dyer. Mine your own view: Self-supervised learning through across-sample prediction. Feb. 2021.
- [4] S. Ben-David, J. Blitzer, K. Crammer, A. Kulesza, F. Pereira, and J. W. Vaughan. A theory of learning from different domains. *Machine Learning*, 79(1-2):151–175, oct 2009.
- [5] S. Ben-David, J. Blitzer, K. Crammer, and F. Pereira. Analysis of representations for domain adaptation. In B. Schölkopf, J. Platt, and T. Hoffman, editors, *Advances in Neural Information Processing Systems*, volume 19. MIT Press, 2006.
- [6] A. R. Chambers and S. Rumpel. A stable brain from unstable components: Emerging concepts and implications for neural computation. *Neuroscience*, 357:172–184, Aug. 2017.
- [7] T. Chen, S. Kornblith, M. Norouzi, and G. Hinton. A simple framework for contrastive learning of visual representations. Feb. 2020.
- [8] T. Chen, S. Kornblith, K. Swersky, M. Norouzi, and G. Hinton. Big self-supervised models are strong semi-supervised learners. June 2020.
- [9] C. Clopath, T. Bonhoeffer, M. Hübener, and T. Rose. Variance and invariance of neuronal long-term representations. *Philosophical transactions of the Royal Society of London. Series B, Biological sciences*, 372(1715):20160161, Mar. 2017.
- [10] M. R. Cohen and J. H. R. Maunsell. A neuronal population measure of attention predicts behavioral performance on individual trials. *The Journal of neuroscience : the official journal of the Society for Neuroscience*, 30:15241–15253, Nov. 2010.
- [11] T. Comito. *Touch of Evil: Orson Welles, Director*. Rutgers films in print. Rutgers University Press, 1985.
- [12] S. E. J. de Vries, J. A. Lecoq, M. A. Buice, P. A. Groblewski, G. K. Ocker, M. Oliver, D. Feng, N. Cain, P. Ledochowitsch, D. Millman, K. Roll, M. Garrett, T. Keenan, L. Kuan, S. Mihalas, S. Olsen, C. Thompson, W. Wakeman, J. Waters, D. Williams, C. Barber, N. Berbesque, B. Blanchard, N. Bowles, S. D. Caldejon, L. Casal, A. Cho, S. Cross, C. Dang, T. Dolbeare, M. Edwards, J. Galbraith, N. Gaudreault, T. L. Gilbert, F. Griffin, P. Hargrave, R. Howard, L. Huang, S. Jewell, N. Keller, U. Knoblich, J. D. Larkin, R. Larsen, C. Lau, E. Lee, F. Lee, A. Leon, L. Li, F. Long, J. Luviano, K. Mace, T. Nguyen, J. Perkins, M. Robertson, S. Seid, E. Shea-Brown, J. Shi, N. Sjoquist, C. Slaughterbeck, D. Sullivan, R. Valenza, C. White, A. Williford, D. M. Witten, J. Zhuang, H. Zeng, C. Farrell, L. Ng, A. Bernard, J. W. Phillips, R. C. Reid, and C. Koch. A large-scale standardized physiological survey reveals functional organization of the mouse visual cortex. *Nature Neuroscience*, 23(1):138–151, dec 2019.
- [13] D. Deitch, A. Rubin, and Y. Ziv. Representational drift in the mouse visual cortex. *Current Biology*, 31(19):4327–4339.e6, oct 2021.
- [14] J. Deng, W. Dong, R. Socher, L.-J. Li, K. Li, and L. Fei-Fei. Imagenet: A large-scale hierarchical image database. In *2009 IEEE conference on computer vision and pattern recognition*, pages 248–255. Ieee, 2009.
- [15] K. Desai and J. Johnson. Virtex: Learning visual representations from textual annotations. June 2020.

- [16] A. K. Dhawale, R. Poddar, S. B. Wolff, V. A. Normand, E. Kopelowitz, and B. P. Ölveczky. Automated long-term recording and analysis of neural activity in behaving animals. *eLife*, 6, Sept. 2017.
- [17] L. N. Driscoll, N. L. Pettit, M. Minderer, S. N. Chettih, and C. D. Harvey. Dynamic reorganization of neuronal activity patterns in parietal cortex. *Cell*, 170(5):986–999.e16, aug 2017.
- [18] Y. Dubois, B. Bloem-Reddy, K. Ullrich, and C. J. Maddison. Lossy compression for lossless prediction. June 2021.
- [19] T. A. Engel and N. A. Steinmetz. New perspectives on dimensionality and variability from large-scale cortical dynamics. *Current opinion in neurobiology*, 58:181–190, Oct. 2019.
- [20] A. A. Faisal, L. P. J. Selen, and D. M. Wolpert. Noise in the nervous system. *Nature reviews. Neuroscience*, 9:292–303, Apr. 2008.
- [21] C. Fang, H. He, Q. Long, and W. J. Su. Exploring deep neural networks via layer-peeled model: Minority collapse in imbalanced training. *Proceedings of the National Academy of Sciences of the United States of America*, 118, Oct. 2021.
- [22] A. Funamizu, F. Marbach, and A. M. Zador. Stable sound decoding despite modulated sound representation in the auditory cortex. *bioRxiv*, 2023.
- [23] J. A. Gallego, M. G. Perich, R. H. Chowdhury, S. A. Solla, and L. E. Miller. Long-term stability of cortical population dynamics underlying consistent behavior. *Nature neuroscience*, 23:260–270, Feb. 2020.
- [24] M. A. Goodale and A. D. Milner. Separate visual pathways for perception and action. *Trends in neurosciences*, 15:20–25, Jan. 1992.
- [25] M. Gutmann and A. Hyvärinen. Noise-contrastive estimation: A new estimation principle for unnormalized statistical models. In Y. W. Teh and M. Titterton, editors, *Proceedings of the Thirteenth International Conference on Artificial Intelligence and Statistics*, volume 9 of *Proceedings of Machine Learning Research*, pages 297–304, Chia Laguna Resort, Sardinia, Italy, 13–15 May 2010. PMLR.
- [26] L. E. Hallum, M. S. Landy, and D. J. Heeger. Human primary visual cortex (v1) is selective for second-order spatial frequency. *Journal of neurophysiology*, 105:2121–2131, May 2011.
- [27] X. Y. Han, V. Pappas, and D. L. Donoho. Neural collapse under mse loss: Proximity to and dynamics on the central path. June 2021.
- [28] D. J. Heeger. The representation of visual stimuli in primary visual cortex. *Current Directions in Psychological Science*, 3(5):159–163, oct 1994.
- [29] D. Huber, D. A. Gutnisky, S. Peron, D. H. O’Connor, J. S. Wiegert, L. Tian, T. G. Oertner, L. L. Looger, and K. Svoboda. Multiple dynamic representations in the motor cortex during sensorimotor learning. *Nature*, 484:473–478, Apr. 2012.
- [30] D. Jancke, W. Erlhagen, G. Schöner, and H. R. Dinse. Shorter latencies for motion trajectories than for flashes in population responses of cat primary visual cortex. *The Journal of physiology*, 556:971–982, May 2004.
- [31] A. Joulin, L. van der Maaten, A. Jabri, and N. Vasilache. Learning visual features from large weakly supervised data. Nov. 2015.
- [32] J. J. Jun, N. A. Steinmetz, J. H. Siegle, D. J. Denman, M. Bauza, B. Barbarits, A. K. Lee, C. A. Anastassiou, A. Andrei, C. Aydın, M. Barbic, T. J. Blanche, V. Bonin, J. Couto, B. Dutta, S. L. Gratiy, D. A. Gutnisky, M. Häusser, B. Karsh, P. Ledochowitsch, C. M. Lopez, C. Mitelut, S. Musa, M. Okun, M. Pachitariu, J. Putzeys, P. D. Rich, C. Rossant, W.-L. Sun, K. Svoboda, M. Carandini, K. D. Harris, C. Koch, J. O’Keefe, and T. D. Harris. Fully integrated silicon probes for high-density recording of neural activity. *Nature*, 551(7679):232–236, Nov. 2017.

- [33] P. Khosla, P. Teterwak, C. Wang, A. Sarna, Y. Tian, P. Isola, A. Maschinot, C. Liu, and D. Krishnan. Supervised contrastive learning. Apr. 2020.
- [34] A. Krizhevsky, I. Sutskever, and G. E. Hinton. Imagenet classification with deep convolutional neural networks. In F. Pereira, C. Burges, L. Bottou, and K. Weinberger, editors, *Advances in Neural Information Processing Systems*, volume 25. Curran Associates, Inc., 2012.
- [35] S. J. Levy, N. R. Kinsky, W. Mau, D. W. Sullivan, and M. E. Hasselmo. Hippocampal spatial memory representations in mice are heterogeneously stable. *Hippocampus*, 31:244–260, Mar. 2021.
- [36] Y. Livneh and M. L. Andermann. Cellular activity in insular cortex across seconds to hours: Sensations and predictions of bodily states. *Neuron*, 109(22):3576–3593, nov 2021.
- [37] W. Lotter, G. Kreiman, and D. Cox. A neural network trained for prediction mimics diverse features of biological neurons and perception. *Nature machine intelligence*, 2:210–219, Apr. 2020.
- [38] H. Lütcke, D. J. Margolis, and F. Helmchen. Steady or changing? long-term monitoring of neuronal population activity. *Trends in neurosciences*, 36(7):375–384, July 2013.
- [39] E. A. Mankin, G. W. Diehl, F. T. Sparks, S. Leutgeb, and J. K. Leutgeb. Hippocampal ca2 activity patterns change over time to a larger extent than between spatial contexts. *Neuron*, 85:190–201, Jan. 2015.
- [40] T. D. Marks and M. J. Goard. Stimulus-dependent representational drift in primary visual cortex. *Nature Communications*, 12(1), aug 2021.
- [41] T. Marques, M. T. Summers, G. Fioreze, M. Fridman, R. F. Dias, M. B. Feller, and L. Petreanu. A role for mouse primary visual cortex in motion perception. *Current biology : CB*, 28:1703–1713.e6, June 2018.
- [42] D. McAllester and K. Stratos. Formal limitations on the measurement of mutual information. Nov. 2018.
- [43] J. S. Montijn, P. M. Goltstein, and C. M. A. Pennartz. Mouse v1 population correlates of visual detection rely on heterogeneity within neuronal response patterns. *eLife*, 4:e10163, Dec. 2015.
- [44] S. E. Palmer, O. Marre, M. J. Berry, and W. Bialek. Predictive information in a sensory population. *Proceedings of the National Academy of Sciences of the United States of America*, 112:6908–6913, June 2015.
- [45] V. Pappas, X. Y. Han, and D. L. Donoho. Prevalence of neural collapse during the terminal phase of deep learning training. *Proceedings of the National Academy of Sciences*, 117(40):24652–24663, sep 2020.
- [46] V. Pappas, X. Y. Han, and D. L. Donoho. Prevalence of neural collapse during the terminal phase of deep learning training. *Proceedings of the National Academy of Sciences of the United States of America*, 117:24652–24663, Oct. 2020.
- [47] B. Poole, S. Ozair, A. van den Oord, A. A. Alemi, and G. Tucker. On variational bounds of mutual information. May 2019.
- [48] A. Radford, J. W. Kim, C. Hallacy, A. Ramesh, G. Goh, S. Agarwal, G. Sastry, A. Askell, P. Mishkin, J. Clark, G. Krueger, and I. Sutskever. Learning transferable visual models from natural language supervision. Feb. 2021.
- [49] R. P. Rao and D. H. Ballard. Predictive coding in the visual cortex: a functional interpretation of some extra-classical receptive-field effects. *Nature neuroscience*, 2:79–87, Jan. 1999.
- [50] U. Rokni, A. G. Richardson, E. Bizzi, and H. S. Seung. Motor learning with unstable neural representations. *Neuron*, 54:653–666, May 2007.
- [51] Y. Ruan, Y. Dubois, and C. J. Maddison. Optimal representations for covariate shift. Dec. 2021.

- [52] A. Rubin, N. Geva, L. Sheintuch, and Y. Ziv. Hippocampal ensemble dynamics timestamp events in long-term memory. *eLife*, 4, Dec. 2015.
- [53] M. E. Rule, A. R. Loback, D. V. Raman, L. N. Driscoll, C. D. Harvey, and T. O’Leary. Stable task information from an unstable neural population. *eLife*, 9, July 2020.
- [54] S. Sadeh and C. Clopath. Contribution of behavioural variability to representational drift. *eLife*, 11:e77907, aug 2022.
- [55] M. B. Sariyildiz, J. Perez, and D. Larlus. Learning visual representations with caption annotations. Aug. 2020.
- [56] G. E. Schneider. Two visual systems. *Science*, 163(3870):895–902, 1969.
- [57] S. Schneider, J. H. Lee, and M. W. Mathis. Learnable latent embeddings for joint behavioural and neural analysis. *Nature*, May 2023.
- [58] C. E. Schoonover, S. N. Ohashi, R. Axel, and A. J. P. Fink. Representational drift in primary olfactory cortex. *Nature*, 594(7864):541–546, jun 2021.
- [59] C. Schuhmann, R. Vencu, R. Beaumont, R. Kaczmarczyk, C. Mullis, A. Katta, T. Coombes, J. Jitsev, and A. Komatsuzaki. Laion-400m: Open dataset of clip-filtered 400 million image-text pairs. Nov. 2021.
- [60] M. L. Schölvinck, A. B. Saleem, A. Benucci, K. D. Harris, and M. Carandini. Cortical state determines global variability and correlations in visual cortex. *The Journal of neuroscience : the official journal of the Society for Neuroscience*, 35:170–178, Jan. 2015.
- [61] L. Sheintuch, N. Geva, H. Baumer, Y. Rechavi, A. Rubin, and Y. Ziv. Multiple maps of the same spatial context can stably coexist in the mouse hippocampus. *Current biology : CB*, 30:1467–1476.e6, Apr. 2020.
- [62] E. J. Shin, Y. Jang, S. Kim, H. Kim, X. Cai, H. Lee, J. H. Sul, S.-H. Lee, Y. Chung, D. Lee, and M. W. Jung. Robust and distributed neural representation of action values. *eLife*, 10:e53045, apr 2021.
- [63] J. H. Siegle, X. Jia, S. Durand, S. Gale, C. Bennett, N. Graddis, G. Heller, T. K. Ramirez, H. Choi, J. A. Luviano, P. A. Groblewski, R. Ahmed, A. Arkhipov, A. Bernard, Y. N. Billeh, D. Brown, M. A. Buice, N. Cain, S. Caldejon, L. Casal, A. Cho, M. Chvilicek, T. C. Cox, K. Dai, D. J. Denman, S. E. J. de Vries, R. Dietzman, L. Esposito, C. Farrell, D. Feng, J. Galbraith, M. Garrett, E. C. Gelfand, N. Hancock, J. A. Harris, R. Howard, B. Hu, R. Hytnen, R. Iyer, E. Jessett, K. Johnson, I. Kato, J. Kiggins, S. Lambert, J. Lecoq, P. Ledochowitsch, J. H. Lee, A. Leon, Y. Li, E. Liang, F. Long, K. Mace, J. Melchior, D. Millman, T. Mollenkopf, C. Nayan, L. Ng, K. Ngo, T. Nguyen, P. R. Nicovich, K. North, G. K. Ocker, D. Ollerenshaw, M. Oliver, M. Pachitariu, J. Perkins, M. Reding, D. Reid, M. Robertson, K. Ronellenfitch, S. Seid, C. Slaughterbeck, M. Stoecklin, D. Sullivan, B. Sutton, J. Swapp, C. Thompson, K. Turner, W. Wakeman, J. D. Whitesell, D. Williams, A. Williford, R. Young, H. Zeng, S. Naylor, J. W. Phillips, R. C. Reid, S. Mihalas, S. R. Olsen, and C. Koch. Survey of spiking in the mouse visual system reveals functional hierarchy. *Nature*, 592(7852):86–92, jan 2021.
- [64] N. Srivastava and R. R. Salakhutdinov. Multimodal learning with deep boltzmann machines. In F. Pereira, C. Burges, L. Bottou, and K. Weinberger, editors, *Advances in Neural Information Processing Systems*, volume 25. Curran Associates, Inc., 2012.
- [65] T. Strohmer and R. Heath. Grassmannian frames with applications to coding and communication. Jan. 2003.
- [66] M. Subramaniyan, A. S. Ecker, S. S. Patel, R. J. Cotton, M. Bethge, X. Pitkow, P. Berens, and A. S. Tolias. Faster processing of moving compared with flashed bars in awake macaque v1 provides a neural correlate of the flash lag illusion. *Journal of neurophysiology*, 120:2430–2452, Nov. 2018.
- [67] D. Sussillo, R. Jozefowicz, L. F. Abbott, and C. Pandarinath. Lfads - latent factor analysis via dynamical systems. Aug. 2016.

- [68] H. Tan and M. Bansal. Lxmert: Learning cross-modality encoder representations from transformers. Aug. 2019.
- [69] B. Thomee, D. A. Shamma, G. Friedland, B. Elizalde, K. Ni, D. Poland, D. Borth, and L.-J. Li. Yfcc100m: The new data in multimedia research. *Communications of the ACM*, 59(2), pp. 64-73, 2016, Mar. 2015.
- [70] Y. Tian, D. Krishnan, and P. Isola. Contrastive multiview coding. June 2019.
- [71] Y. Tian, Y. Wang, D. Krishnan, J. B. Tenenbaum, and P. Isola. Rethinking few-shot image classification: a good embedding is all you need? Mar. 2020.
- [72] N. Tishby, F. C. Pereira, and W. Bialek. The information bottleneck method. Apr. 2000.
- [73] D. J. Tolhurst, J. A. Movshon, and A. F. Dean. The statistical reliability of signals in single neurons in cat and monkey visual cortex. *Vision research*, 23:775-785, 1983.
- [74] E. M. Trautmann, S. D. Stavisky, S. Lahiri, K. C. Ames, M. T. Kaufman, D. J. O’Shea, S. Vyas, X. Sun, S. I. Ryu, S. Ganguli, and K. V. Shenoy. Accurate estimation of neural population dynamics without spike sorting. *Neuron*, 103(2):292-308.e4, jul 2019.
- [75] A. van den Oord, Y. Li, and O. Vinyals. Representation learning with contrastive predictive coding. July 2018.
- [76] S. Wang, B. Hoshal, E. A. de Laitre, O. Marre, M. Berry, and S. Palmer. Learning low-dimensional generalizable natural features from retina using a u-net. In A. H. Oh, A. Agarwal, D. Belgrave, and K. Cho, editors, *Advances in Neural Information Processing Systems*, 2022.
- [77] T. Wang and P. Isola. Understanding contrastive representation learning through alignment and uniformity on the hypersphere. May 2020.
- [78] L. Wasserman. *All of statistics : a concise course in statistical inference*. Springer, New York, 2010.
- [79] M. Wu, C. Zhuang, D. Yamins, and N. D. Goodman. On the importance of views in unsupervised representation learning. 2020.
- [80] J. Xia, T. D. Marks, M. J. Goard, and R. Wessel. Stable representation of a naturalistic movie emerges from episodic activity with gain variability. *Nature communications*, 12:5170, Aug. 2021.
- [81] D. Yi, S. Musall, A. Churchland, N. Padilla-Coreano, and S. Saxena. Disentangled multi-subject and social behavioral representations through a constrained subspace variational autoencoder (CS-VAE). sep 2022.
- [82] Z. A. Zayyad, J. H. R. Maunsell, and J. N. MacLean. Normalization in mouse primary visual cortex. *bioRxiv : the preprint server for biology*, Apr. 2023.
- [83] R. Zhang, P. Isola, and A. A. Efros. Split-brain autoencoders: Unsupervised learning by cross-channel prediction. Nov. 2016.
- [84] Y. Zhang, H. Jiang, Y. Miura, C. D. Manning, and C. P. Langlotz. Contrastive learning of medical visual representations from paired images and text. Oct. 2020.
- [85] D. Zhou and X.-X. Wei. Learning identifiable and interpretable latent models of high-dimensional neural activity using pi-vae. *NeurIPS 2020*, Nov. 2020.
- [86] Z. Zhu, T. Ding, J. Zhou, X. Li, C. You, J. Sulam, and Q. Qu. A geometric analysis of neural collapse with unconstrained features. May 2021.
- [87] Y. Ziv, L. D. Burns, E. D. Cocker, E. O. Hamel, K. K. Ghosh, L. J. Kitch, A. E. Gamal, and M. J. Schnitzer. Long-term dynamics of CA1 hippocampal place codes. *Nature Neuroscience*, 16(3):264-266, feb 2013.